GDCh

Research Articles

Angewandte
Chemie
International Edition
www.angewandte.org

Covalent Organic Frameworks

A Nanographene-Based Two-Dimensional Covalent Organic Framework as a Stable and Efficient Photocatalyst

Enquan Jin, Shuai Fu, Hiroki Hanayama, Matthew A. Addicoat, Wenxin Wei, Qiang Chen, Robert Graf, Katharina Landfester, Mischa Bonn, Kai A. I. Zhang,* Hai I. Wang,* Klaus Müllen,* and Akimitsu Narita*

Abstract: Synthesis of covalent organic frameworks (COFs) with desirable organic units furnishes advanced materials with unique functionalities. As an emerging class of two-dimensional (2D) COFs, sp²-carbon-conjugated COFs provide a facile platform to build highly stable and crystalline porous polymers. Herein, a 2D olefin-linked COF was prepared by employing nanographene, namely, dibenzo-[hi,st]ovalene (DBOV), as a building block. The DBOV-COF exhibits unique ABC-stacked lattices, enhanced stability, and charge-carrier mobility of ≈0.6 cm² V⁻¹ s⁻¹ inferred from ultrafast terahertz photoconductivity measurements. The ABC-stacking structure was revealed by the high-resolution transmission electron microscopy and powder X-ray diffraction. DBOV-COF demonstrated remarkable photocatalytic activity in hydroxylation, which was attributed to the exposure of narrow-energy-gap DBOV cores in the COF pores, in conjunction with efficient charge transport following light absorption.

Introduction

The construction of fully conjugated two-dimensional (2D) covalent organic frameworks (COFs) through topologically directed polycondensation of rationally predesigned building blocks provides a facile platform with which to generate functional porous materials for optoelectronic and hetero-catalytic applications.[1] By employing thermodynamically controlled and defect-repairing processes involving reversi-

ble or partially reversible bond formation, numerous 2D COFs with extended π-conjugation have been developed, including vinylene-linked highly crystalline structures with outstanding stability and photocatalytic properties.[2] However, most of these lattices possess layered structures with AA stacking, which hampers heterocatalytic efficiency because the active sites eclipse each other.[3] Although attempts at changing stacking modes by introducing steri-cally demanding substituents have been reported for imine-linked COFs,[4] the achievement of ABC stacking with 2D vinylene-linked COFs has remained elusive. Their successful formation with highly ordered structures presumably depends on the preassembly of monomers and oligomers through π–π interactions, which are disturbed by large substituents. Therefore, the choice of the functionalized monomeric building block needs to ensure a proper balance between steric and π–π bonding effects for both kinetic and thermodynamic control.

Nanographenes, polycyclic aromatic hydrocarbons (PAHs) with sizes above 1 nm, are considered as promising candidates for next-generation semiconductors with discrete and tunable energy gaps.[5] In the past decade, myriad nanographenes with attractive optical,[6] electronic[7] and magnetic[8] properties have been developed. In particular, we reported dibenzo[*hi,st*]ovalene (DBOV) derivatives with both zigzag and armchair edges, which exhibit intense absorption of visible light over a broad wavelength domain, high stability, and brilliant red fluorescence with quantum yields up to 97%.[9] Moreover, properly functionalized

[*] Dr. E. Jin, S. Fu, W. Wei, Dr. Q. Chen, Dr. R. Graf,
Prof. Dr. K. Landfester, Prof. Dr. M. Bonn, Prof. Dr. K. A. I. Zhang,
Dr. H. I. Wang, Prof. Dr. K. Müllen, Prof. Dr. A. Narita
Max Planck Institute for Polymer Research
Ackermannweg 10, 55128, Mainz (Germany)
E-mail: wanghai@mpip-mainz.mpg.de
muellen@mpip-mainz.mpg.de
narita@mpip-mainz.mpg.de

Dr. H. Hanayama, Prof. Dr. A. Narita
Organic and Carbon Nanomaterials Unit
Okinawa Institute of Science and Technology Graduate University
Kunigami-gun, Okinawa 904-0495 (Japan)
E-mail: akimitsu.narita@oist.jp

Prof. Dr. K. Müllen
Department of Chemistry
Johannes Gutenberg University Mainz
Duesbergweg 10–14, 55128 Mainz (Germany)

Prof. Dr. M. A. Addicoat
School of Science and Technology
Nottingham Trent University
Clifton Lane, Nottingham, NG11 8NS (UK)

Prof. Dr. K. A. I. Zhang
Department of Materials Science
Fudan University
Shanghai 200433 (P.R. China)
E-mail: kai_zhang@fudan.edu.cn

DBOV adopts a crystal structure with pronounced intermolecular π–π interactions.[10] These intriguing features prompted us to introduce DBOV into a 2D vinylene-linked COF skeleton with a packing mode different from AA stacking.

In this work, we synthesized an olefin-linked 2D COF with ABC stacking by employing 6,14-bis(4-formyl-2,6-dimethylphenyl)dibenzo[*hi,st*]ovalene (DBOV-CHO) as the building block. The resulting DBOV-COF combines high crystallinity and chemical stability with strong light-harvesting ability over a broad absorption domain and high charge-carrier mobility, and has an ABC-stacking structure that is expected to allow guest molecules to effectively access the active sites.[4] Remarkably, with these key features, DBOV-COF could serve as an efficient photocatalyst for the hydroxylation of aromatic boronic acids to phenols under visible light irradiation.

Results and Discussion

Synthesis of DBOV-COF: DBOV-CHO was synthesized by adapting our previous synthetic protocol,[9a] as described in the Supporting Information. Polymerization of C_2-symmetric DBOV-CHO and 3,5-dicyano-2,4,6-trimethylpyridine (DCTMP) under optimized solvothermal conditions with piperidine catalysis provided a deep blue-colored 2D DBOV-COF in quantitative yield as a highly crystalline powder (see the Supporting Information, Figure 1a). Through washing with *n*-hexylamine in chlorobenzene, well purified DBOV-COF could be obtained (Figure S1). Other

reaction conditions, for example, utilizing mixtures of dimethylacetamide (DMAc) and 1,2-dichlorobenzene (ODCB) (v/v=1/1) as the solvent instead of DMAc, generated DBOV-based conjugated microporous polymers (DBOV-CMPs) with amorphous structures based on powder X-ray diffraction (PXRD) analysis (see the Supporting Information).

The chemical structure of the obtained vinylene-linked DBOV-COF was analyzed by different spectroscopic and microscopic methods (Figures S2–S5). Fourier transform infrared (FTIR) spectroscopy revealed the occurrence of polymerization, which was evidenced by the band at 2223 cm^{-1} corresponding to the stretching vibration of the C≡N substituent and by the disappearance of the aldehyde band at 2720 cm^{-1} (Figure S2). The appearance of a new peak at 1625 cm^{-1}, which could be assigned to the *trans*-HC=CH stretching vibration, supported the formation of the vinylene linkage (Figure S2). The formation of DBOV-COF was also confirmed by ^{13}C cross-polarization/magic angle spinning (CP/MAS) solid-state nuclear magnetic resonance (NMR) spectroscopy (Figure S3). Solid-state ^{13}C NMR spectra of DBOV-COF confirm the successful polycondensation of DBOV-CHO and DCTMP monomers, as evidenced by the disappearance of the peak at 189 ppm assigned to the carbon atoms of the aldehyde groups, and the peaks at 22 ppm and 24 ppm from the two methyl groups of DCTMP. The solid-state NMR signals of DBOV-COF are significantly broadened compared to those of DBOV-CHO, suggesting strong variations of the local molecular packing arrangement after the COF formation. It is thus unfortunately not possible to assign the ^{13}C CP/MAS NMR
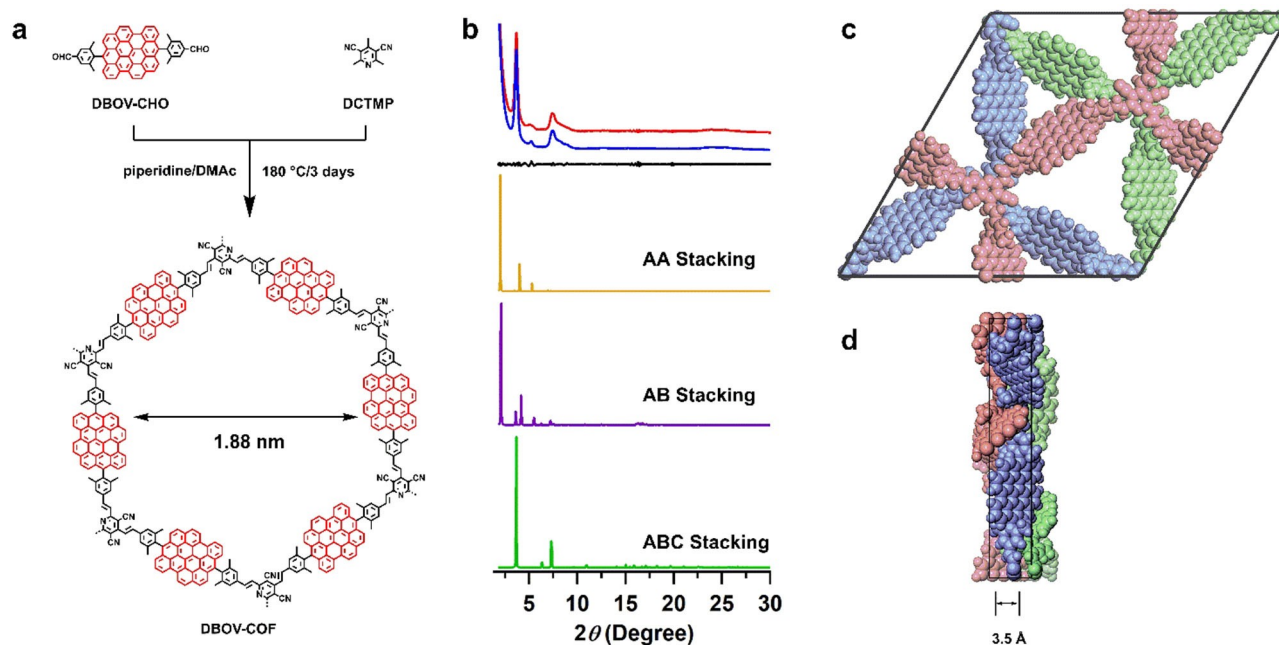

Figure 1. a) Topology-directed synthesis of an olefin-linked DBOV-COF with a pore size of 1.88 nm. b) Experimentally observed PXRD pattern of the DBOV-COF (red curve), the Pawley refinement (blue curve) and their difference (black curve), as well as simulated patterns for the AA-stacking mode (orange curve), AB-stacking mode (purple curve) and ABC-stacking mode (green curve). c, d) Rebuilt crystal structure of the (c) top and (d) side views with an interlayer distance of 3.5 Å along the z-direction.

signals in the aromatic range of DBOV-COF to specific aromatic carbon atoms of the DBOV core and vinylene linkages. On the other hand, the NMR signals are observed in the same range as those of DBOV-CHO, supporting the retainment of the DBOV structure inside the COF. It is noted that NMR signals from carbon atoms inside the DBOV core are strongly reduced in intensity by the CP/MAS method based on polarization transfer from protons in close spatial proximity. Additionally, field-emission scanning electron microscopy (FE-SEM) revealed a flake-like morphology of DBOV-COF (Figure S4), and thermogravimetric analysis (TGA) demonstrated its high thermal stability, with no weight loss occurring until 420 °C under a nitrogen atmosphere (Figure S5).

Crystal Structure Simulation: PXRD indicated a crystalline structure of the obtained DBOV-COF; Peaks at 3.68°, 4.82°, 7.38°, 11.27°, and 24.83° were assigned to the (110), (300), (220), (330), and (001) facets, respectively (Figure 1b, red curve). The packing structures of DBOV-COF were simulated by density functional theory (DFT) tight-binding calculations, followed by the generation of the corresponding PXRD patterns.[11] Among the various possible stacking types, the ABC stacking mode (Table S3) yielded a PXRD pattern (Figure 1b, green curve) in good agreement with the experimentally observed pattern. The Pawley refined PXRD pattern (Figure 1b, blue curve), generated using the $P1$ space group (Table S4) with unit-cell parameters of $a = 48.1910$ Å, $b = 48.7242$ Å, $c = 6.8537$ Å, $\alpha = \beta = 90°$, and $\gamma = 120°$ from the ABC-stacking model (see the Supporting Information for details), reproduced the experimental curve, as is evident from the negligible differences between the two ($R_{wp} = 0.32\%$ and $R_p = 0.19\%$, Figure 1b, black curve). The presence of the peak corresponding to the (001) facet suggested that the layers aligned along the third dimension perpendicular to the 2D sheets (Figure 1c,d).[1b] Based on the peak position, the interlayer distance was calculated to be 3.5 Å. By contrast, the simulated XRD profiles of the AA- and AB-stacking modes (Figure 1b, orange, and purple curves, respectively; see Tables S5 and S6 for the atomistic coordinates) did not match the experimentally measured PXRD pattern.

DBOV-COF produced reversible nitrogen sorption isotherms, in line with the expected porous framework (Figure 2a). The Brunauer–Emmett–Teller (BET) surface area was evaluated to be 581 m^{2}g^{-1}. The pore size distribution was determined with nonlocal density functional theory (NLDFT), indicating that DBOV-COF had a microporous structure with a discrete pore size of 1.9 nm (Figure 2b). This result is consistent with the simulated model of the DBOV-COF crystal (Figure 1a and c).

Electron Microscopic Analysis: High-resolution transmission electron microscopic (HR-TEM) analysis further confirmed the successful formation of 2D DBOV-COF. As in the previous report on olefin-linked COFs,[3a] the DBOV-COF was stable for at least a few seconds under standard electron dose for TEM observation. A periodic pattern was observed, as shown in Figure 3a, from a thin-film structure exfoliated in dichloromethane (Figure S6a). The average distance obtained from a plot profile (2.44 ± 0.06 nm, Fig-
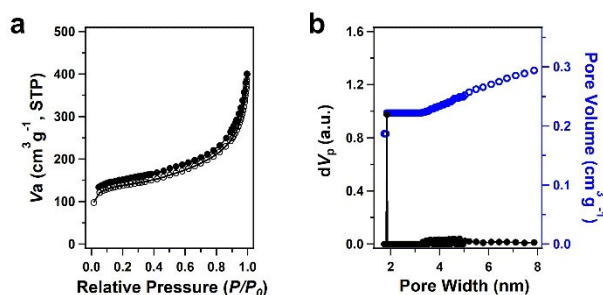

Figure 2. Nitrogen sorption isotherms of DBOV-COF measured at 77 K. a) Absorption (open symbols) and desorption curves (closed symbols). b) Pore size distribution and pore volume profiles based on NLDFT calculation.
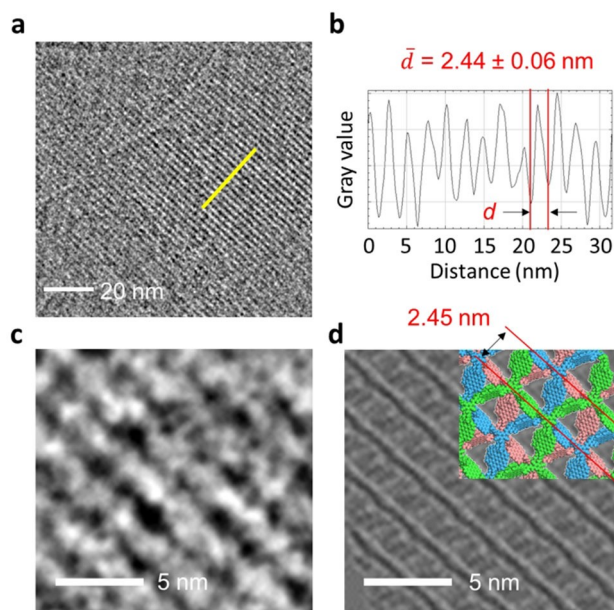

Figure 3. TEM characterizations of DBOV-COF. a) HR-TEM image of DBOV-COF, showing the periodic structure. b) The plot profile along the yellow line in (a). c) Enlarged HR-TEM image and d) an image simulated for DBOV-COF. Molecular model in ABC-stacking (three layers are colored red, green, and blue) is partially overlaid.

ure 3b) corresponds to the spacing of the parallel DBOV units in the ABC-stacking model (2.45 nm, Figure 3d, red lines). Figure 3c and d show an enlarged TEM image and an image simulated for ABC-stacked films of DBOV-COF with an inclination of ≈18° at the same scale. As shown in the overlaid image of TEM and simulation (Figure S6c), the characteristic stripe pattern was well reproduced in the simulation. The simulation indicates that the linear contrasts are composed of a combination of DBOV units in each of the three layers in ABC-stacking (colored red, green, and blue in the model, Figure 3d). Two other potential stacking modes (AA, AB) would show a very different contrast (Figure S6d), which strongly supports the ABC-stacking of the obtained DBOV-COF.

Chemical Stability: The stability of DBOV-COF was examined by soaking powder samples in the following

Angew. Chem. Int. Ed. **2022**, 61, e202114059 (3 of 8)

© 2021 The Authors. Angewandte Chemie International Edition published by Wiley-VCH GmbH

solvents for one month: *N,N*-dimethylformamide (DMF), dimethyl sulfoxide (DMSO), water, and concentrated aqueous solutions of HCl (12 M) and NaOH (14 M). According to the weights of the residual samples (Figure 4a), the stability against organic solvents was outstanding with little weight loss (<5 wt%). The weight losses were still small (
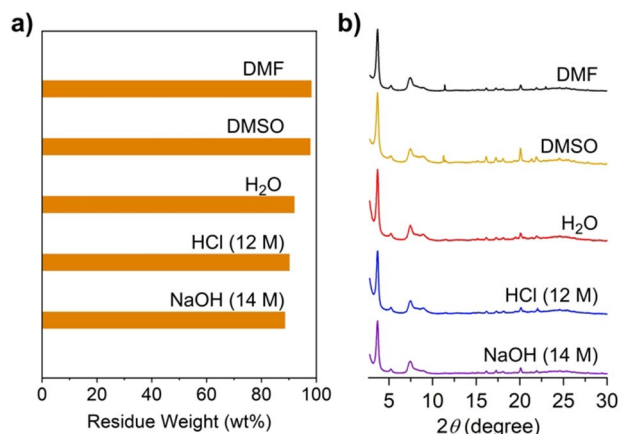
$\approx$10 wt%), even in water, concentrated HCl, and NaOH solutions. Furthermore, the peak positions and signal intensities of the PXRD patterns after soaking in these solvents were almost unchanged (Figure 4b). These results highlighted the exceptionally high chemical stability of DBOV-COF.

Electronic Structure Characterization: The solid-state diffuse reflectance spectra measured on a powder sample of DBOV-COF showed broadband absorption from 300 nm to 800 nm, which covered the absorption regions of DBOV-CHO and DCTMP (Figure 5a, red, blue, and black curves, respectively). The optical band gap was estimated to be 1.74 eV according to the Kubelka–Munk-transformed reflectance spectra (Figure 5b). Cyclic voltammetry (CV) analysis of DBOV-COF (Figure S7) revealed an oxidation potential of −0.33 V, corresponding to the energy of the valence band maximum (VBM) at −4.47 eV.

DFT calculations (Figure S8) helped to evaluate the band structure and the partial density of states (PDOS), suggesting an indirect band gap of 1.27 eV. The PDOS result indicates that both the conduction band minimum (CBM) of −4.97 eV and the VBM of −3.70 eV originate from the π-delocalization of the *2p* orbital of the C atoms. The simulated band gap is slightly smaller than the experimental result. This is expected, as DFT calculations typically underestimate band gaps.[12]

Photoconductivity and Charge-Carrier Transport: To investigate the electrical properties of DBOV-COF, we measured the time- and frequency-resolved photoconductivity employing optical-pump THz-probe (OPTP) spectroscopy on a powder-based thin film ($\approx$200 μm thickness) sandwiched between two fused silica substrates. OPTP spectroscopy is a purely optical method that measures photoconductivity and quantifies the intrinsic charge-carrier mobility of samples in a contact-free fashion. Figure 5c shows the photoconductivity dynamics of DBOV-COF following 3.1 eV photoexcitation. An ultrafast, sub-ps rise in the real part of the photoconductivity is attributed to the optical generation of free charge carriers. This is followed by biexponential decay with an average carrier lifetime (*t*) of $\approx$8 ps (determined by weighting the slow and fast decay contributions), which could be attributed to the loss of mobile carriers as a result of localization (e.g., trapping to localized states or forming bound excitons) and/or electron-hole recombination.[13]

Figure 5d presents the frequency-resolved complex THz photoconductivity of DBOV-COF at $\approx$3 ps after photoexcitation. The spectral response could be well fitted by the Drude–Smith model[14] (see the Supporting Information for details), which depicted the conduction of free charge carriers subject to a preferential backscattering effect due to the presence of, e.g., grain boundaries and variations in the structural configuration. The degree of backscattering is quantified by a parameter *c* spanning from 0 (for Drude-like transport) to −1 (for localized charges with 100% backscattering). The best fit to the data yielded a Drude–Smith scattering time (*τ*) of 36±6 fs and a *c* parameter of −0.85± 0.02. Using the effective mass *m** from DFT calculations (see the Supporting Information for details, Figure S8), the

Figure 4. a) Residual weight of DBOV-COF after soaking in DMF (98%), DMSO (97%), H$_2$O (92%), HCl (12 M, 90%) and NaOH (14 M, 89%) for one month, and b) PXRD patterns of DBOV-COF after immersion in the different solvents.
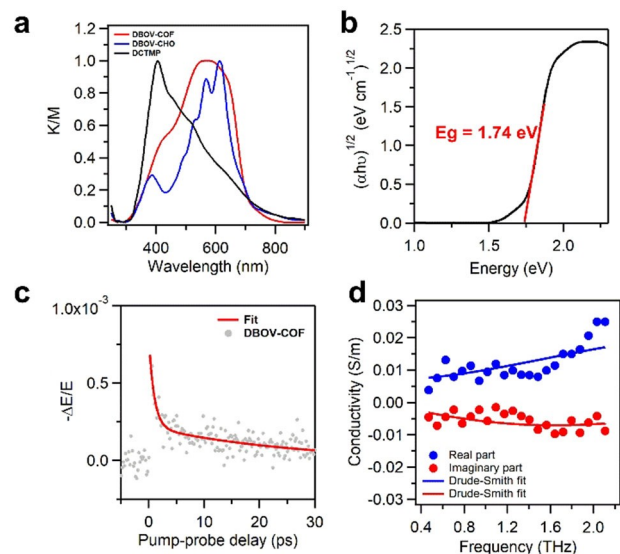

Figure 5. Optical and electronic properties of DBOV-COF. a) Solid-state UV/Vis diffuse reflectance spectra (DBOV-COF, red curve; DBOV-CHO, blue curve and DCTMP, black curve). b) The Kubelka–Munk-transformed reflectance spectra. c) Time-resolved photoconductivity dynamics for DBOV-COF. The samples were photoexcited by a pulsed laser with a duration of $\approx$50 fs, photon energy of 3.1 eV, and an incident photon density of 4.1×10^{15} cm^{-2}. The photoconductivity $\Delta\sigma$ is proportional to the change in the transmitted THz electrical field ($-\Delta E/E$) following photoexcitation. The red solid line represents a bi-exponential fit to the decay. d) Frequency-resolved complex photoconductivity of DBOV-COF at $\approx$3 ps after photoexcitation. The solid lines are the Drude–Smith fits to the data, as discussed in the main text and Supporting Information.

charge-carrier mobility in the dc limit for DBOV-COF was estimated to be 0.6 ± 0.1 cm^{2}V^{-1}s^{-1}. The estimated mobility is reasonably high on the basis of comparison to the previously reported values for other state-of-the-art conductive metal-free COFs, which were determined with the same or similar photoconductivity measurements and range from ≈0.014 to ≈8 cm^{2}V^{-1}s^{-1}.[15] Such high charge-carrier mobility enables effective transport of photogenerated carriers towards[16] catalytically active sites in DBOV-COF and thus may play a role in facilitating the photocatalytic process.

Photocatalytic Properties: The broad absorption range, high chemical stability, and high charge-carrier mobility of DBOV-COF motivated us to investigate the possible application of DBOV-COF as a photocatalyst. This is particularly relevant for the hydroxylation reaction since the energy levels of DBOV-COF appeared suitable for transferring photogenerated electrons to oxygen.[17] We thus chose the transformation of 2-naphthylboronic acid to 2-naphthol as the model reaction, with oxygen gas as the oxidant, triethylamine (TEA) as the sacrificial agent, and acetonitrile as the solvent under visible light irradiation at room temperature. In view of the broad absorption of DBOV-COF, we selected a low-power white LED lamp (0.07 W cm^{-2}) as a light source instead of a commonly used xenon lamp (300 W). After 5 h of photoirradiation, 2-naphthol was isolated in an excellent yield of 97 % (Table 1, entry 4), while the absence of either DBOV-COF, light, or oxygen resulted in trace yields (Table 1, entries 1–3). In marked contrast to DBOV-COF, both DBOV-CHO and DCTMP monomers showed much lower photocatalytic performance with limited reaction yields of 20.6 % and 11.9 %, respectively (Table 1, entries 5,6).

To evaluate the critical role of the DBOV unit, imine-linked TFPPy-PDA-COF with pyrene-based porous structures[18] and olefin-linked amorphous py-DCTMP-CMP

(see the Supporting Information for details) were prepared as control COF samples. In sharp contrast to the results with DBOV-COF, both TFPPy-PDA-COF and py-DCTMP-CMP showed limited catalytic activity, giving only 28 % yield and trace amounts, respectively, of the hydroxylated product (Table 1, entries 7 and 8).

A *p*-terphenyl-based g-C$_{40}$N$_3$-COF[3a] was also prepared for comparison, but the product yield was only 13 % (Table 1, entry 9). On the other hand, amorphous DBOV-CMP resulted in a 46 % product yield (Table 1, entry 10), which was significantly lower than the product yield with DBOV-COF. All these results indicated that the ordered lattice structure is a prerequisite for the excellent catalytic function of DBOV-COF and highlighted the relevance of DBOV as a unique photocatalytic component of COFs, in stark contrast to smaller PAHs typically used to fabricate COFs.
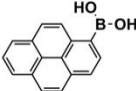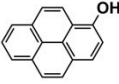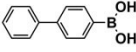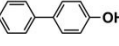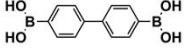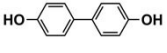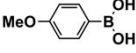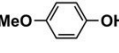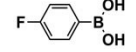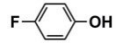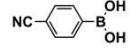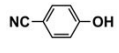
The high photocatalytic activity of DBOV-COF could also be demonstrated for various other arylboronic acids, including 1-pyrenylboronic acid, 4-biphenylboronic acid, and 4,4′-biphenyldiboronic acid (Table 2, entries 1–3). Substrates with electron-withdrawing groups resulted in lower yields, but 4-cyano- and 4-nitrobenzeneboronic acids could be hydroxylated to the corresponding phenols in 89 % and 85 % yields, respectively (Table 2, entries 6 and 7). Figure S9 shows a proposed reaction mechanism for the photocatalytic process, based on the literature.[19] 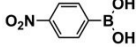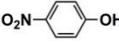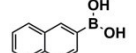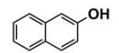We have performed an additional control experiment by implementing 5,5-dimethyl-1-pyrroline-*N*-oxide (DMPO) as a superoxide radical trapping agent, and the EPR analysis demonstrated a typical pattern characteristic for DMPO-O$_2^{\bullet-}$ adducts (Fig-

Table 1: Screening and control reaction conditions for the photocatalytic hydroxylation of 2-naphthylboronic acid.[a]

Entry	Photocatalyst	Visible light	O$_2$	Yield [%][b]
1	none	+	+	trace
2	DBOV-COF	−	+	trace
3	DBOV-COF	+	−	trace
4	DBOV-COF	+	+	97
5	DBOV-CHO	+	+	20.6
6	DCTMP	+	+	11.9
7	TFPPy-PDA-COF	+	+	28
8	Py-DCTMP-CMP	+	+	trace
9	g-C$_{40}$N$_3$-COF	+	+	13
10	DBOV-CMP	+	+	46
11	DBOV-COF (+1,4-benzoquinone)	+	+	8.6
12	DBOV-COF (+KI)	+	+	3.7

[a] Reaction conditions: 2-naphthylboronic acid (0.5 mmol), TEA (1.5 mmol), photocatalyst (1 mg mL^{-1}), CH$_3$CN (3 mL), O$_2$ (1 atm), 5 h white LED lamp (0.07 W cm^{-2}). [b] Isolated yield.

Table 2: Photocatalytic hydroxylation of various arylboronic acids using DBOV-COF as photocatalyst.[a]

Entry	Substrate	Product	t [h]	Yield [%][b]
1			5	97
2			5	98
3			5	88
4			5	96
5			5	93
6			5	89
7			5	85
8			5	97

[a] Reaction conditions: arylboronic acid (0.5 mmol), DBOV-COF (1 mg mL^{-1}), Et$_3$N (1.5 mmol), white LED illumination (0.07 W cm^{-2}), O$_2$ (1 atm), CH$_3$CN (3 mL). [b] Isolated yield.

ure S10).[20] The photocatalytic performance of DBOV-COF significantly decreased in the presence of 1,4-benzoquinone as the electron scavenger or KI as the hole scavenger. This observation further supports the proposed mechanism of photocatalytic hydroxylation (Table 1, entries 11,12). As an olefin-linked stable heterogeneous photocatalyst, DBOV-COF could be readily recovered by filtration and directly reused after washing with tetrahydrofuran and acetone. Even after 8 cycles of reaction and recovery, no significant decay was observed in the reaction yields (Figure S11) or crystallinity (Figure S12) of DBOV-COF, which further indicated the robustness of its ordered frameworks. Finally, we investigated the hydroxylation of 2-naphthylboronic acid catalyzed by DBOV-COF and recorded a time-dependent conversion plot (Figure S13). The turnover frequency (TOF) was estimated to be $1.6 \times 10^{-2}\,\mathrm{s}^{-1}$, which was higher than those reported for other COFs (see Table S2).

We have also performed photocatalytic reductive dehalogenation of α-bromoacetophenone (Scheme S3) and photoredox borylation of diazonium salt to boronic ester (Scheme S4) with DBOV-COF as the photocatalyst. The yields were higher than 90 % in both reactions. These results demonstrate the general applicability of the DBOV-COFs as photocatalysts for different types of organic reactions, including reduction (Scheme S3) and redox reactions (Scheme S4).

Compared with previously reported COFs as photosensitizers for the hydroxylation of arylboronic acids (Table S2),[3d,19] DBOV-COF provided oxidation with higher yields, shorter irradiation times, and smaller loading amounts. The photocatalytic performance largely depends on the light-harvesting and photon-to-electron conversion ability of the catalyst. It is thus also notable that DBOV-COF demonstrated high catalytic performance with an apparent quantum yield (AQY) of 9.73 % upon irradiation under a low-power LED lamp with a wavelength of 620 nm (see the Supporting Information for more details),[20] highlighting the excellent light-harvesting ability of DBOV-COF.

In porous catalysts, photoexcited electrons need to quickly move to the interfaces with guest molecules for efficient photocatalysis while minimizing hole-electron recombination.[21] As shown by THz spectroscopy, the efficient charge-carrier transport along the highly ordered lattice of DBOV-COF and the relatively long charge carrier lifetime of 8 ps most likely play key roles in determining its high photocatalytic performance. This is in contrast to py-DCTMP-CMP and DBOV-CMP, which have amorphous structures that may cause fast trapping of charge carriers and rapid hole-electron recombination. Moreover, the extraordinary ABC-stacked layered structure of DBOV-COF with its large "open" π-surface can presumably increase the access of arylboronic acids as guest molecules together with oxygen molecules that are supposed to be initially reduced by the transfer of photogenerated electrons.[19] Theoretical calculation (Figure S14) indicates that both VBM and CBM locate on the DBOV units in DBOV-COF, which most probably serve as the effective photocatalytic sites. Therefore, the superior features of

DBOV-COF for photocatalytic hydroxylation can be summarized as i) a marked light-harvesting ability, ii) a reasonably high charge-carrier mobility within an ordered framework and iii) large exposed interfaces.

Conclusion

In summary, a DBOV-based ABC-stacked 2D COF was synthesized with robust olefin linkages. The COF exhibited unique structural and electrical properties, as demonstrated by PXRD, HR-TEM, and THz spectroscopy. When employed as a photocatalyst, DBOV-COF efficiently promoted the hydroxylation of aromatic boronic acids to hydroxylated arenes with stable cycling performance. This work provides a facile strategy for introducing various functional nanographenes to the world of COFs to achieve unprecedented structures and properties, e.g., enhanced photocatalytic activity. The use of nanographenes, with tunable energy levels and gaps, as building blocks of COFs, could also direct research toward hitherto elusive photocatalytic processes.

Acknowledgements

Conflict of Interest

The authors declare no conflict of interest.

Keywords: ABC stacking · Covalent organic framework · Nanographene · Photocatalyst · THz spectroscopy

[1] a) S. Lin, C. S. Diercks, Y.-B. Zhang, N. Kornienko, E. M. Nichols, Y. Zhao, A. R. Paris, D. Kim, P. Yang, O. M. Yaghi, C. J. Chang, *Science* **2015**, *349*, 1208–1213; b) K. Geng, T. He, R. Liu, S. Dalapati, K. T. Tan, Z. Li, S. Tao, Y. Gong, Q. Jiang, D. Jiang, *Chem. Rev.* **2020**, *120*, 8814–8933; c) D. Bessinger, L. Ascherl, F. Auras, T. Bein, *J. Am. Chem. Soc.* **2017**, *139*, 12035–12042; d) S.-Y. Ding, J. Gao, Q. Wang, Y. Zhang, W.-G.

Angew. Chem. Int. Ed. **2022**, *61*, e202114059 (6 of 8)

© 2021 The Authors. Angewandte Chemie International Edition published by Wiley-VCH GmbH

Song, C.-Y. Su, W. Wang, *J. Am. Chem. Soc.* **2011**, *133*, 19816–19822; e) X. Wang, L. Chen, S. Y. Chong, M. A. Little, Y. Wu, W.-H. Zhu, R. Clowes, Y. Yan, M. A. Zwijnenburg, R. S. Sprick, A. I. Cooper, *Nat. Chem.* **2018**, *10*, 1180–1189; f) M. Bhadra, S. Kandambeth, M. K. Sahoo, M. Addicoat, E. Balaraman, R. Banerjee, *J. Am. Chem. Soc.* **2019**, *141*, 6152–6156; g) V. S. Vyas, F. Haase, L. Stegbauer, G. Savasci, F. Podjaski, C. Ochsenfeld, B. V. Lotsch, *Nat. Commun.* **2015**, *6*, 8508; h) J. W. Colson, W. R. Dichtel, *Nat. Chem.* **2013**, *5*, 453–465; i) Z. Mi, P. Yang, R. Wang, J. Unruangsri, W. Yang, C. Wang, J. Guo, *J. Am. Chem. Soc.* **2019**, *141*, 14433–14442; j) Q. Sun, Y. Tang, B. Aguila, S. Wang, F.-S. Xiao, P. K. Thallapally, A. M. Al-Enizi, A. Nafady, S. Ma, *Angew. Chem. Int. Ed.* **2019**, *58*, 8670–8675; *Angew. Chem.* **2019**, *131*, 8762–8767.

[2] a) H. Lyu, C. S. Diercks, C. Zhu, O. M. Yaghi, *J. Am. Chem. Soc.* **2019**, *141*, 6848–6852; b) X. Zhuang, W. Zhao, F. Zhang, Y. Cao, F. Liu, S. Bi, X. Feng, *Polym. Chem.* **2016**, *7*, 4176–4181; c) E. Jin, M. Asada, Q. Xu, S. Dalapati, M. A. Addicoat, M. A. Brady, H. Xu, T. Nakamura, T. Heine, Q. Chen, D. Jiang, *Science* **2017**, *357*, 673–676; d) E. Jin, Z. Lan, Q. Jiang, K. Geng, G. Li, X. Wang, D. Jiang, *Chem* **2019**, *5*, 1632–1647; e) S. Xu, G. Wang, B. P. Biswal, M. Addicoat, S. Paasch, W. Sheng, X. Zhuang, E. Brunner, T. Heine, R. Berger, X. Feng, *Angew. Chem. Int. Ed.* **2019**, *58*, 849–853; *Angew. Chem.* **2019**, *131*, 859–863; f) S. Wei, F. Zhang, W. Zhang, P. Qiang, K. Yu, X. Fu, D. Wu, S. Bi, F. Zhang, *J. Am. Chem. Soc.* **2019**, *141*, 14272–14279; g) A. Acharjya, L. Longworth-Dunbar, J. Roeser, P. Pachfule, A. Thomas, *J. Am. Chem. Soc.* **2020**, *142*, 14033–14038; h) J. Xu, C. Yang, S. Bi, W. Wang, Y. He, D. Wu, Q. Liang, X. Wang, F. Zhang, *Angew. Chem. Int. Ed.* **2020**, *59*, 23845–23853; *Angew. Chem.* **2020**, *132*, 24053–24061; i) C. Yuan, S. Fu, K. Yang, B. Hou, Y. Liu, J. Jiang, Y. Cui, *J. Am. Chem. Soc.* **2021**, *143*, 369–381.

[3] a) S. Bi, C. Yang, W. Zhang, J. Xu, L. Liu, D. Wu, X. Wang, Y. Han, Q. Liang, F. Zhang, *Nat. Commun.* **2019**, *10*, 2467; b) Y. Zhao, H. Liu, C. Wu, Z. Zhang, Q. Pan, F. Hu, R. Wang, P. Li, X. Huang, Z. Li, *Angew. Chem. Int. Ed.* **2019**, *58*, 5376–5381; *Angew. Chem.* **2019**, *131*, 5430–5435; c) R. Chen, J.-L. Shi, Y. Ma, G. Lin, X. Lang, C. Wang, *Angew. Chem. Int. Ed.* **2019**, *58*, 6430–6434; *Angew. Chem.* **2019**, *131*, 6496–6500; d) S. Bi, P. Thiruvengadam, S. Wei, W. Zhang, F. Zhang, L. Gao, J. Xu, D. Wu, J.-S. Chen, F. Zhang, *J. Am. Chem. Soc.* **2020**, *142*, 11893–11900; e) Z. Fu, X. Wang, A. M. Gardner, X. Wang, S. Y. Chong, G. Neri, A. J. Cowan, L. Liu, X. Li, A. Vogel, R. Clowes, M. Bilton, L. Chen, R. S. Sprick, A. I. Cooper, *Chem. Sci.* **2020**, *11*, 543–550.

[4] X. Wu, X. Han, Y. Liu, Y. Liu, Y. Cui, *J. Am. Chem. Soc.* **2018**, *140*, 16124–16133.

[5] a) A. Narita, X.-Y. Wang, X. Feng, K. Müllen, *Chem. Soc. Rev.* **2015**, *44*, 6616–6643; b) J. Liu, X. Feng, *Angew. Chem. Int. Ed.* **2020**, *59*, 23386–23401; *Angew. Chem.* **2020**, *132*, 23591–23607; c) Z. Sun, Q. Ye, C. Chi, J. Wu, *Chem. Soc. Rev.* **2012**, *41*, 7857–7889; d) M. Di Giovannantonio, A. Keerthi, J. I. Urgel, M. Baumgarten, X. Feng, P. Ruffieux, A. Narita, R. Fasel, K. Müllen, *J. Am. Chem. Soc.* **2020**, *142*, 1721–1725; e) K. Kawasumi, Q. Zhang, Y. Segawa, L. T. Scott, K. Itami, *Nat. Chem.* **2013**, *5*, 739–744; f) M. Stępień, E. Gońka, M. Żyła, N. Sprutta, *Chem. Rev.* **2017**, *117*, 3479–3716.

[6] a) Y. Hu, G. M. Paternò, X.-Y. Wang, X.-C. Wang, M. Guizzardi, Q. Chen, D. Schollmeyer, X.-Y. Cao, G. Cerullo, F. Scotognella, K. Müllen, A. Narita, *J. Am. Chem. Soc.* **2019**, *141*, 12797–12803; b) C. M. Cruz, S. Castro-Fernández, E. Maçôas, J. M. Cuerva, A. G. Campaña, *Angew. Chem. Int. Ed.* **2018**, *57*, 14782–14786; *Angew. Chem.* **2018**, *130*, 14998–15002; c) Y. Gu, R. Muñoz-Mármol, S. Wu, Y. Han, Y. Ni, M. A. Díaz-García, J. Casado, J. Wu, *Angew. Chem. Int. Ed.* **2020**, *59*, 8113–8117; *Angew. Chem.* **2020**, *132*, 8190–8194; d) C. M. Cruz,

I. R. Márquez, I. F. A. Mariz, V. Blanco, C. Sánchez-Sánchez, J. M. Sobrado, J. A. Martín-Gago, J. M. Cuerva, E. Maçôas, A. G. Campaña, *Chem. Sci.* **2018**, *9*, 3917–3924; e) H.-A. Lin, Y. Sato, Y. Segawa, T. Nishihara, N. Sugimoto, L. T. Scott, T. Higashiyama, K. Itami, *Angew. Chem. Int. Ed.* **2018**, *57*, 2874–2878; *Angew. Chem.* **2018**, *130*, 2924–2928; f) D. Lu, G. Zhuang, H. Wu, S. Wang, S. Yang, P. Du, *Angew. Chem. Int. Ed.* **2017**, *56*, 158–162; *Angew. Chem.* **2017**, *129*, 164–168.

[7] a) C. Rogers, C. Chen, Z. Pedramrazi, A. A. Omrani, H.-Z. Tsai, H. S. Jung, S. Lin, M. F. Crommie, F. R. Fischer, *Angew. Chem. Int. Ed.* **2015**, *54*, 15143–15146; *Angew. Chem.* **2015**, *127*, 15358–15361; b) Z.-S. Wu, Y.-Z. Tan, S. Zheng, S. Wang, K. Parvez, J. Qin, X. Shi, C. Sun, X. Bao, X. Feng, K. Müllen, *J. Am. Chem. Soc.* **2017**, *139*, 4506–4512; c) J. Cao, Y.-M. Liu, X. Jing, J. Yin, J. Li, B. Xu, Y.-Z. Tan, N. Zheng, *J. Am. Chem. Soc.* **2015**, *137*, 10914–10917; d) H.-A. Lin, Y. Kato, Y. Segawa, L. T. Scott, K. Itami, *Chem. Sci.* **2019**, *10*, 2326–2330; e) M. M. Martin, D. Lungerich, P. Haines, F. Hampel, N. Jux, *Angew. Chem. Int. Ed.* **2019**, *58*, 8932–8937; *Angew. Chem.* **2019**, *131*, 9027–9032.

[8] a) Y. Zheng, C. Li, C. Xu, D. Beyer, X. Yue, Y. Zhao, G. Wang, D. Guan, Y. Li, H. Zheng, C. Liu, J. Liu, X. Wang, W. Luo, X. Feng, S. Wang, J. Jia, *Nat. Commun.* **2020**, *11*, 607; b) S. Mishra, D. Beyer, K. Eimre, J. Liu, R. Berger, O. Gröning, C. A. Pignedoli, K. Müllen, R. Fasel, X. Feng, P. Ruffieux, *J. Am. Chem. Soc.* **2019**, *141*, 10621–10625; c) S. Mishra, D. Beyer, R. Berger, J. Liu, O. Gröning, J. I. Urgel, K. Müllen, P. Ruffieux, X. Feng, R. Fasel, *J. Am. Chem. Soc.* **2020**, *142*, 1147–1152; d) W. Zeng, T. Y. Gopalakrishna, H. Phan, T. Tanaka, T. S. Herng, J. Ding, A. Osuka, J. Wu, *J. Am. Chem. Soc.* **2018**, *140*, 14054–14058; e) Z. Zeng, S. Lee, J. L. Zafra, M. Ishida, X. Zhu, Z. Sun, Y. Ni, R. D. Webster, R.-W. Li, J. T. López Navarrete, C. Chi, J. Ding, J. Casado, D. Kim, J. Wu, *Angew. Chem. Int. Ed.* **2013**, *52*, 8561–8565; *Angew. Chem.* **2013**, *125*, 8723–8727.

[9] a) Q. Chen, S. Thoms, S. Stöttinger, D. Schollmeyer, K. Müllen, A. Narita, T. Basché, *J. Am. Chem. Soc.* **2019**, *141*, 16439–16449; b) Q. Chen, D. Schollmeyer, K. Müllen, A. Narita, *J. Am. Chem. Soc.* **2019**, *141*, 19994–19999; c) G. M. Paternò, L. Nicoli, Q. Chen, K. Müllen, A. Narita, G. Lanzani, F. Scotognella, *J. Phys. Chem. C* **2018**, *122*, 25007–25013; d) X. Liu, S.-Y. Chen, Q. Chen, X. Yao, M. Gelléri, S. Ritz, S. Kumar, C. Cremer, K. Landfester, K. Müllen, S. H. Parekh, A. Narita, M. Bonn, *Angew. Chem. Int. Ed.* **2020**, *59*, 496–502; *Angew. Chem.* **2020**, *132*, 504–510; e) Q. Chen, W. Zajaczkowski, J. Seibel, S. De Feyter, W. Pisula, K. Müllen, A. Narita, *J. Mater. Chem. C* **2019**, *7*, 12898–12906.

[10] Q. Chen, D. Wang, M. Baumgarten, D. Schollmeyer, K. Müllen, A. Narita, *Chem. Asian J.* **2019**, *14*, 1703–1707.

[11] a) B. Aradi, B. Hourahine, T. Frauenheim, *J. Phys. Chem. A* **2007**, *111*, 5678–5684; b) www.dftb.org.

[12] D. Bagayoko, *AIP Adv.* **2014**, *4*, 127104.

[13] a) J. Nyakuchena, S. Ostresh, D. Streater, B. Pattengale, J. Neu, C. Fiankor, W. Hu, E. D. Kinigstein, J. Zhang, X. Zhang, C. A. Schmuttenmaer, J. Huang, *J. Am. Chem. Soc.* **2020**, *142*, 21050–21058; b) A. Tries, S. Osella, P. Zhang, F. Xu, C. Ramanan, M. Kläui, Y. Mai, D. Beljonne, H. I. Wang, *Nano Lett.* **2020**, *20*, 2993–3002; c) F. Xu, C. Yu, A. Tries, H. Zhang, M. Kläui, K. Basse, M. R. Hansen, N. Bilbao, M. Bonn, H. I. Wang, Y. Mai, *J. Am. Chem. Soc.* **2019**, *141*, 10972–10977.

[14] N. V. Smith, *Phys. Rev. B* **2001**, *64*, 155106.

[15] H. Sahabudeen, H. Qi, M. Ballabio, M. Položij, S. Olthof, R. Shivhare, Y. Jing, S. Park, K. Liu, T. Zhang, J. Ma, B. Rellinghaus, S. Mannsfeld, T. Heine, M. Bonn, E. Cánovas, Z. Zheng, U. Kaiser, R. Dong, X. Feng, *Angew. Chem. Int. Ed.* **2020**, *59*, 6028–6036; *Angew. Chem.* **2020**, *132*, 6084–6092.

[16] Y. Su, Z. Yao, F. Zhang, H. Wang, Z. Mics, E. Cánovas, M. Bonn, X. Zhuang, X. Feng, *Adv. Funct. Mater.* **2016**, *26*, 5893–5902.

[17] Z. J. Wang, R. Li, K. Landfester, K. A. I. Zhang, *Polymer* **2017**, *126*, 291–295.

[18] E. Jin, K. Geng, K. H. Lee, W. Jiang, J. Li, Q. Jiang, S. Irle, D. Jiang, *Angew. Chem. Int. Ed.* **2020**, *59*, 12162–12169; *Angew. Chem.* **2020**, *132*, 12260–12267.

[19] a) P.-F. Wei, M.-Z. Qi, Z.-P. Wang, S.-Y. Ding, W. Yu, Q. Liu, L.-K. Wang, H.-Z. Wang, W.-K. An, W. Wang, *J. Am. Chem. Soc.* **2018**, *140*, 4623–4631; b) M. Wang, Y. Na, M. Gorlov, L. Sun, *Dalton Trans.* **2009**, 6458–6467.

[20] W. Huang, N. Huber, S. Jiang, K. Landfester, K. A. I. Zhang, *Angew. Chem. Int. Ed.* **2020**, *59*, 18368–18373; *Angew. Chem.* **2020**, *132*, 18526–18531.

[21] a) G. Zhang, Z.-A. Lan, X. Wang, *Angew. Chem. Int. Ed.* **2016**, *55*, 15712–15727; *Angew. Chem.* **2016**, *128*, 15940–15956; b) T. Banerjee, F. Podjaski, J. Kröger, B. P. Biswal, B. V. Lotsch, *Nat. Rev. Mater.* **2021**, *6*, 168–190; c) M. Zhang, M. Lu, Z.-L. Lang, J. Liu, M. Liu, J.-N. Chang, L.-Y. Li, L.-J. Shang, M. Wang, S.-L. Li, Y.-Q. Lan, *Angew. Chem. Int. Ed.* **2020**, *59*, 6500–6506; *Angew. Chem.* **2020**, *132*, 6562–6568.